



Article

One-Pot Synthesis of Alumina-Titanium Diboride Composite Powder at Low Temperature

Xueyin Liu ¹, Ke Bao ², Junfeng Chen ³, Quanli Jia ⁴  and Shaowei Zhang ^{2,*} ¹ College of Civil Engineering and Architecture, Quzhou University, Quzhou 324000, China; kklldliu@163.com² College of Engineering, Mathematics and Physical Sciences, University of Exeter, Exeter EX4 4QF, UK; kb357@exeter.ac.uk³ The State Key Laboratory of Refractories and Metallurgy, Wuhan University of Science and Technology, Wuhan 430081, China; chenjunfengref@163.com⁴ Henan Key Laboratory of High Temperature Functional Ceramics, Zhengzhou University, Zhengzhou 450052, China; jiaquanli@zzu.edu.cn

* Correspondence: s.zhang@exeter.ac.uk

Abstract: Alumina-titanium diboride (Al₂O₃-TiB₂) composite powders were synthesised via aluminothermic reduction of TiO₂ and B₂O₃, mediated by a molten chloride salt (NaCl, KCl, or MgCl₂). The effects of salt type, initial batch composition, and firing temperature/time on the phase formation and overall reaction extent were examined. Based on the results and equilibrium thermodynamic calculations, the mechanisms underpinning the reaction/synthesis processes were clarified. Given their evaporation losses at test temperatures, appropriately excessive amounts of Al and B₂O₃ are needed to complete the synthesis reaction. Following this, phase-pure Al₂O₃-TiB₂ composite powders composed of 0.3–0.6 μm Al₂O₃ and 30–60 nm TiB₂ particles were successfully fabricated in NaCl after 5 h at 1050 °C. By increasing the firing temperature to 1150 °C, the time required to complete the synthesis reaction could be reduced to 4 h, although the sizes of Al₂O₃ and TiB₂ particles in the resultant phase pure composite powder increased slightly to 1–2 μm and 100–200 nm, respectively.

Keywords: alumina; titanium diboride; composite powder; molten salt synthesis; aluminothermic reduction; boron oxide; titania; thermodynamic calculation



Citation: Liu, X.; Bao, K.; Chen, J.; Jia, Q.; Zhang, S. One-Pot Synthesis of Alumina-Titanium Diboride Composite Powder at Low Temperature. *Materials* **2021**, *14*, 4742. <https://doi.org/10.3390/ma14164742>

Academic Editor: A. Javier Sanchez-Herencia

Received: 16 June 2021
Accepted: 14 August 2021
Published: 22 August 2021

Publisher's Note: MDPI stays neutral with regard to jurisdictional claims in published maps and institutional affiliations.



Copyright: © 2021 by the authors. Licensee MDPI, Basel, Switzerland. This article is an open access article distributed under the terms and conditions of the Creative Commons Attribution (CC BY) license (<https://creativecommons.org/licenses/by/4.0/>).

1. Introduction

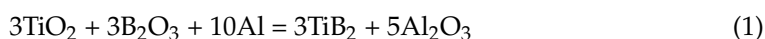
Alumina (Al₂O₃) is a representative high performance ceramic material possessing numerous superior properties. Apart from its high melting point, it exhibits high hardness and mechanical strength, excellent wear and chemical resistances, as well as good electrical/thermal insulation [1]. These, along with its ready availability, make Al₂O₃ an attractive ceramic material applicable to a wide range of structural and functional applications, in, e.g., wear-resistant components, high-speed cutting tools, armors, refractory linings/crucibles, electrical and chemical insulators, and artificial hip joints [2–4]. Unfortunately, it suffers from low fracture toughness and poor thermal shock resistance [5,6], negatively affecting its service performance and life. One of the commonly adopted strategies for overcoming this is to make a composite [7], by combining it with another reinforcement phase, e.g., particles/platelets, or fibrous phases such as carbon fibres and carbon nanotubes. Titanium diboride (TiB₂) stood out as one of the reinforcement phases, owing to its good structural and thermodynamic compatibility with Al₂O₃ [8,9] and its excellent properties such as high melting point, high hardness/elastic modulus, relatively low density, and good thermal/electrical conductivities [10]. Previous studies found that incorporation of TiB₂ particles into Al₂O₃ conferred much improved hardness, strength, fracture toughness and electrical conductivity on the resultant Al₂O₃-TiB₂ composite materials [11–16], making them suitable for a variety of demanding applications, e.g., in electrodes, cutting tools, wear parts, lightweight armors, high-temperature/glow-plug heaters, and heat exchangers [14,17,18].

To fabricate high performance Al_2O_3 - TiB_2 composites, it is key to prepare and use high quality counterpart powders. Conventionally, such composite powders were prepared by directly mixing pre-synthesised TiB_2 and Al_2O_3 powders in a ball mill [11,12,14–17,19,20]. Unfortunately, the final bulk composites exhibited unsatisfactory service performance arising mainly from poor dispersion and distribution of TiB_2 in Al_2O_3 . To overcome this, in-situ formation of the two constituent phases was suggested [21]. For example, a self-propagating high-temperature synthesis (SHS) method was attempted to form in-situ Al_2O_3 and TiB_2 from powder mixtures of Al, TiO_2/Ti , and $\text{B}_2\text{O}_3/\text{B}/\text{H}_3\text{BO}_3$ [18,22–32]. However, this method suffered from several weaknesses; in particular, difficulties to control the synthesis process and synthesise phase pure materials. Apart from SHS, mechanochemical synthesis [8,9,33–35], and milling assisted sol-gel process [36] were investigated. With these two techniques, a long processing time was required, and the resultant powders were often heavily agglomerated, and contaminated during prolonged milling.

In recent years, our group has successfully synthesised several ultra-high temperature boride powders via magnesiothermic reduction of oxide precursors in a molten salt [37–39]. In this work, such a molten salt synthesis (MSS) technique was further developed to synthesise high-quality Al_2O_3 - TiB_2 composite powders at relatively low temperatures. The effects of processing factors such as salt type, initial batch composition, and firing temperature/time on the synthesis process were examined, and the synthesis conditions optimised. Based on the results, and thermodynamic calculations, the mechanisms underpinning the reaction/synthesis process were proposed.

2. Materials and Methods

The TiO_2 ($\geq 99\%$, 100–300 nm), B_2O_3 (99.98%) and Al (99.5%, $\sim 44 \mu\text{m}$) powders were used as the main starting materials, along with KCl ($>99\%$), NaCl ($>99\%$) and anhydrous MgCl_2 ($>98\%$). All of these materials except for Al (Alfa Aesar, Lancashire, UK) were from Sigma-Aldrich (Gillingham, UK). The three main starting materials were mixed in stoichiometric (indicated by the overall Reaction (1)) or nonstoichiometric proportions (with excess Al and B_2O_3), in a mortar and pestle, and further combined with 5 times (by weight) of each of the salts. The final powder mix was contained in an alumina crucible and heated in an argon protected tube furnace to a temperature between 850 and 1150 °C and held for 4–6 h. After cooling to room temperature, the reacted powder coexisting with the residual salt was subjected to repeated hot water washing. The remaining salt-free product powder was dried overnight at 80 °C before being subjected to detailed characterisations.



Phase formation and reaction extent in samples were evaluated based on their X-ray diffraction (XRD) spectra recorded by an X-ray diffractometer (D8 Advance, Bruker, Germany) operated at 40 mA/40 kV (using $\text{CuK}\alpha$ radiation), and at a scan rate of 2° (2 θ) min^{-1} , and the ICDD cards used are: TiB_2 (35-741), Al_2O_3 (corundum) (10-173), Ti_2O_3 (43-1033), Al_3Ti (37-1449), $\text{Al}_{18}\text{B}_4\text{O}_{33}$ (32-3), and MgAl_2O_4 (21-1152). Samples were also gold- or carbon-coated for further microstructural examinations using a scanning electron microscope (SEM, Nova 600, FEI, Hillsboro, OR, USA) and a transmission electron microscope (TEM, JEM 2100, JEOL, Tokyo, Japan), linked with energy-dispersive X-ray spectroscopy (EDS, Oxford Instrument, Oxford, UK).

To assist in clarification of the mechanisms underpinning the whole reaction/synthesis process, thermodynamic calculations were carried out using the commercial FactSage package [40]. The Gibbs energy values for each of the intermediate reactions and the overall reaction (Reaction (1)), as a function of temperature, were calculated.

3. Results and Preliminary Discussion

3.1. Influence of Salt Type on Al_2O_3 - TiB_2 Formation

Figure 1 shows XRD patterns of stoichiometric samples after 4 h firing in different salts at 850 °C. After firing in KCl, α - Al_2O_3 and TiB_2 were identified as the primary phases

in the sample (Figure 1a). Some intermediate $\text{Al}_{18}\text{B}_4\text{O}_{33}$ and Al_3Ti were also detected, along with a trace of Ti_2O_3 , indicating the low extents of Reaction (1) and Al_2O_3 - TiB_2 formation. Replacing KCl with NaCl (Figure 1b) led to an evident increase in the relative peak heights of both Al_2O_3 and TiB_2 , and a decrease in those of Al_3Ti , while those of intermediate $\text{Al}_{18}\text{B}_4\text{O}_{33}$ and Ti_2O_3 changed little, demonstrating the enhanced extents of Al_2O_3 - TiB_2 formation, and the better effect of NaCl than KCl on accelerating the overall reaction. As discussed previously [37–39], several processing parameters—in particular, the solubility and mobility of reaction species in the molten salt—play crucial roles in MSS. Unfortunately, these key processing parameters are not available, so it is difficult to figure out the reasons behind the better accelerating effect of NaCl in the present case. When NaCl was replaced with MgCl_2 , the peak heights of Al_2O_3 and TiB_2 further increased (Figure 1c), and no $\text{Al}_{18}\text{B}_4\text{O}_{33}$, Al_3Ti or Ti_2O_3 was detected, suggesting much enhanced extents of Reaction (1). Nevertheless, an undesirable by-product phase, magnesium aluminate spinel (MgAl_2O_4), was formed in this case, due to likely the reaction between the formed Al_2O_3 and the MgCl_2 (Reaction (2) [41]). In the three cases, except for α - Al_2O_3 , no other transition aluminas were detected at such a low firing temperature. The reason for this was not clear, but it could be due to the locally enhanced salt bath temperature arising from the exothermic reactions, as suggested by the thermodynamic calculations presented later (see Section 4 below). Given the better accelerating effect of NaCl than KCl, and the formation of undesired by-product MgAl_2O_4 in the case of using MgCl_2 , NaCl was chosen specifically to form a liquid reaction medium for the following MSS investigations.

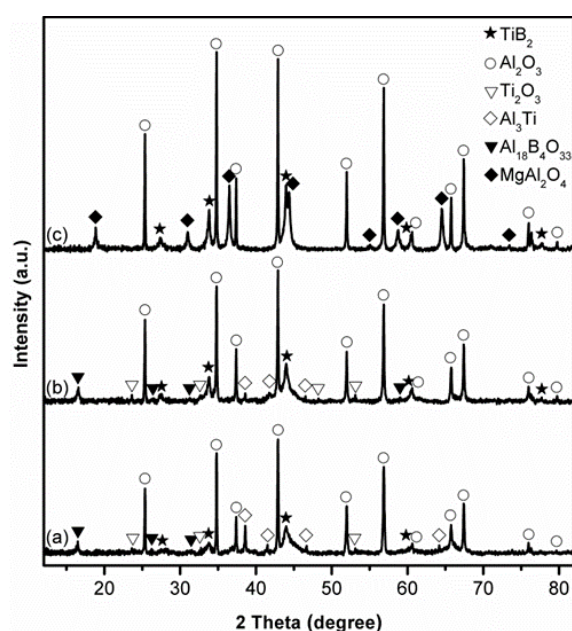
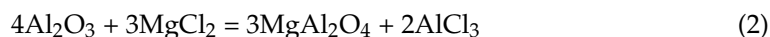


Figure 1. XRD patterns of stoichiometric samples after 4 h firing at 850 °C in: (a) KCl, (b) NaCl, and (c) MgCl_2 .

3.2. Influence of Firing Temperature on Al_2O_3 - TiB_2 Formation

Figure 2 presents XRD patterns of stoichiometric samples after 4 h firing in NaCl at different temperatures. At 850 °C, as already described above, Al_2O_3 and TiB_2 were formed as the primary phases, but some intermediate $\text{Al}_{18}\text{B}_4\text{O}_{33}$, Al_3Ti and Ti_2O_3 were detected (Figure 2a/ Figure 1b). Upon increasing the temperature to 950 (Figure 2b) and 1050 °C (Figure 2c), the relative peak heights of Al_2O_3 and TiB_2 increased significantly. Meanwhile, Al_3Ti disappeared, and Ti_2O_3 changed little, but the peak heights of $\text{Al}_{18}\text{B}_4\text{O}_{33}$ increased. These results implied that increasing the firing temperature favoured not

only the Al_2O_3 - TiB_2 formation but also the $\text{Al}_{18}\text{B}_4\text{O}_{33}$ formation. Further increasing the temperature to $1150\text{ }^\circ\text{C}$ led to a further increase in the peak heights of $\text{Al}_{18}\text{B}_4\text{O}_{33}$ and Ti_2O_3 but decrease in those of Al_2O_3 and TiB_2 (Figure 2d), indicating the adverse effect of such further temperature increase on the Al_2O_3 - TiB_2 formation. This, according to our previous studies on MSS of transition metal borides [37–39], was due to probably evaporation loss of Al at relatively high reaction temperatures [42]. To confirm this, the influence of using excess Al on the Al_2O_3 - TiB_2 formation was further investigated, as described and discussed next.

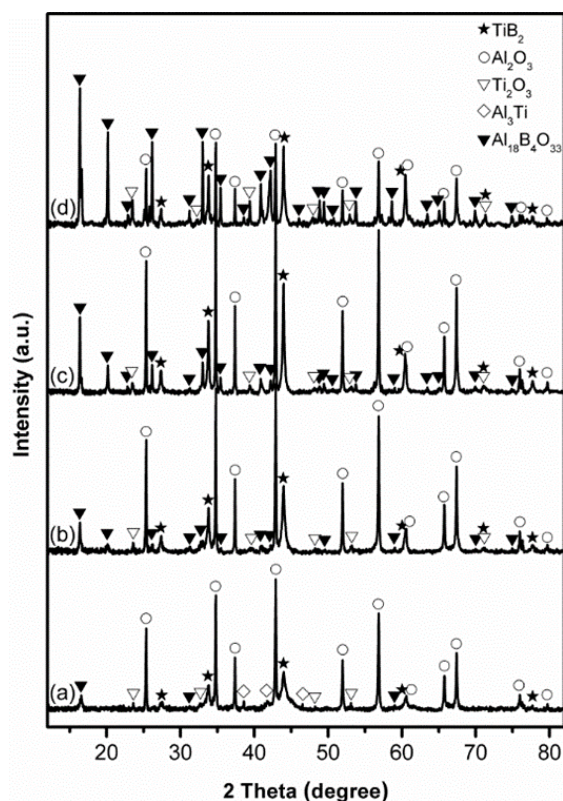


Figure 2. XRD patterns of stoichiometric samples after 4 h firing in NaCl at: (a) 850, (b) 950, (c) 1050, and (d) $1150\text{ }^\circ\text{C}$.

3.3. Influence of Excess Al on Al_2O_3 - TiB_2 Formation

Figure 3 illustrates the influence of excess Al on phase evolution in samples after 4 h firing in NaCl at $1150\text{ }^\circ\text{C}$. The use of 20 wt% more Al resulted in considerable increase in the peak heights of Al_2O_3 and TiB_2 and decrease in those of $\text{Al}_{18}\text{B}_4\text{O}_{33}$ and Ti_2O_3 (Figure 3a,b). By further increasing excess Al to 25 wt%, the peak heights of Al_2O_3 and TiB_2 were further increased. Meanwhile, Ti_2O_3 was completely eliminated, and only minor $\text{Al}_{18}\text{B}_4\text{O}_{33}$ remained (Figure 3c), illustrating positive effects from the Al compensation. Nevertheless, the formation of phase-pure Al_2O_3 - TiB_2 was still not achieved.

To eliminate $\text{Al}_{18}\text{B}_4\text{O}_{33}$, the excess Al was further increased to 30 wt%. Unfortunately, some Al_3Ti was formed instead (Figure 3d), implying that there was no sufficient supply of B in the system, due to probably evaporation loss of B_2O_3 at such a relatively high temperature [43,44].

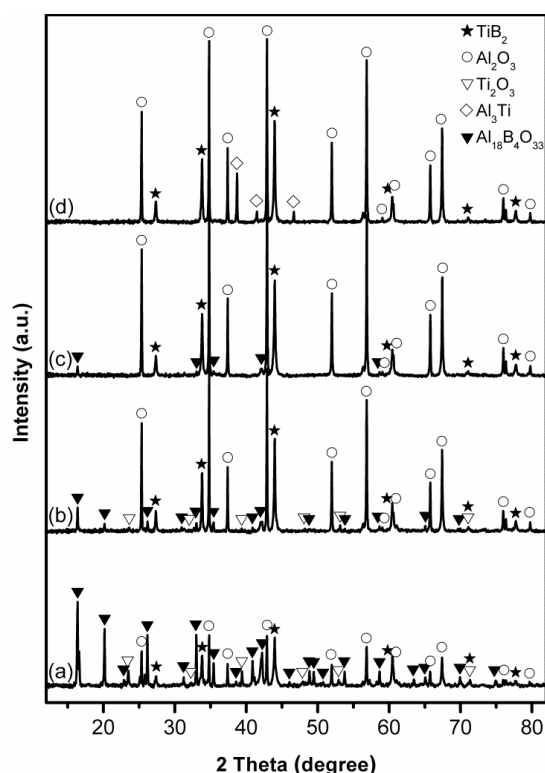


Figure 3. XRD patterns of samples using (a) 0, (b) 20, (c) 25, and (d) 30 wt% excess Al, after 4 h firing in NaCl at 1150 °C.

3.4. Influence of Excess B_2O_3 on Al_2O_3 - TiB_2 Formation

To confirm and address the issue with B_2O_3 evaporation loss, the influence of using excess B_2O_3 (along with 30 wt% excess Al) on the Al_2O_3 - B_2O_3 formation in the sample fired at 1150 °C for 4 h was further investigated as an example. When 10 wt% excess B_2O_3 was used, the peak heights of both Al_2O_3 and TiB_2 increased, whereas those of Al_3Ti decreased considerably (Figure 4b), compared with in the case of stoichiometric sample (Figure 4a). Further increasing the excess B_2O_3 to 20 wt% led to complete elimination of Al_3Ti , and the formation of phase pure Al_2O_3 - TiB_2 (Figure 4c).

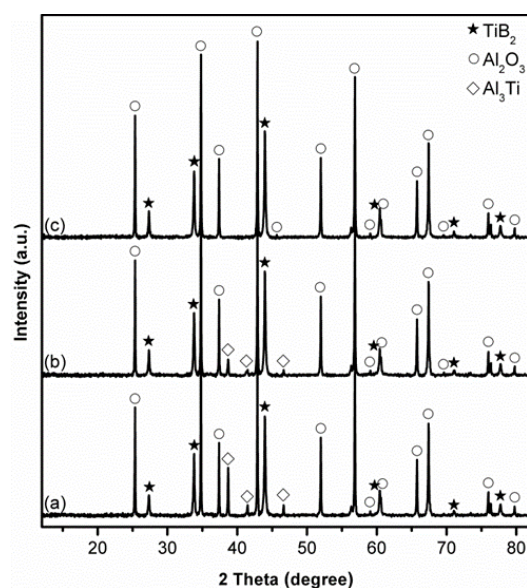


Figure 4. Influence of excess B_2O_3 on phase formation in samples using 30 wt% excess Al, after 4 h firing in NaCl at 1150 °C: (a) 0 (stoichiometric), (b) 10, and (c) 20 wt% excess B_2O_3 .

3.5. Influence of Firing Time on $\text{Al}_2\text{O}_3\text{-TiB}_2$ Formation and Further Optimisation of Synthesis Condition

To reveal the influence of firing time on the $\text{Al}_2\text{O}_3\text{-TiB}_2$ formation and further optimise the synthesis condition, samples containing 30 wt% excess Al and 20 wt% excess B_2O_3 were fired in NaCl at 1050 °C for different time periods, and then analysed by XRD (Figure 5). As shown in Figure 5a,b, with increasing the time at 1050 °C from 4 to 5 h, $\text{Al}_{18}\text{B}_4\text{O}_{33}$ disappeared, whereas the peak heights of Al_3Ti increased. Further extending the time to 6 h resulted in little change in the XRD pattern (Figure 5c), and Al_3Ti was still detected. This, as mentioned above (Section 3.4), indicated that 20 wt% excess B_2O_3 might not be sufficient to compensate for the evaporation loss of B_2O_3 under this condition, in other words, more excess B_2O_3 had to be used. As verified by Figure 6, increasing excess B_2O_3 from 20 wt% to 25 wt% led to significant decrease in the peak heights of Al_3Ti , and further increasing the excess amount to 30 wt%, all the intermediate phases including Al_3Ti disappeared, and phase pure $\text{Al}_2\text{O}_3\text{-TiB}_2$ powder was finally obtained.

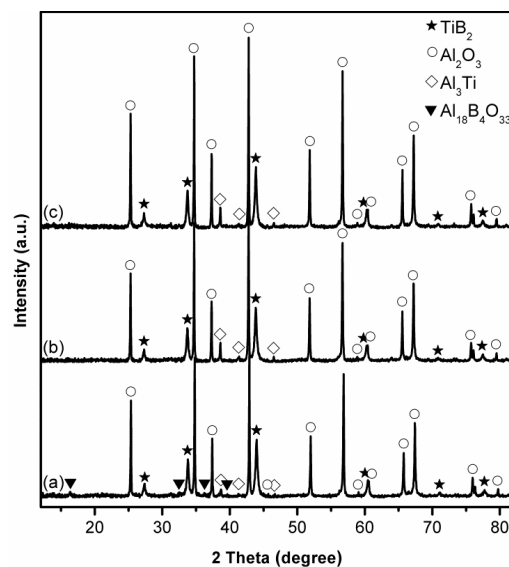


Figure 5. XRD patterns of samples using 30 wt% excess Al and 20 wt% excess B_2O_3 after firing in NaCl at 1050 °C for: (a) 4, (b) 5, and (c) 6 h.

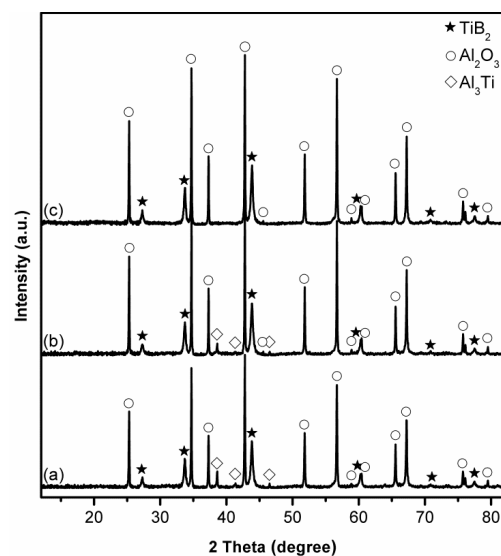


Figure 6. XRD patterns of samples after firing in NaCl at 1050 °C for 5 h using 30 wt% excess Al, and (a) 20, (b) 25, and (c) 30 wt% excess B_2O_3 .

3.6. Microstructure of $\text{Al}_2\text{O}_3\text{-TiB}_2$ Product Powder

As demonstrated in Figures 4c and 6c and discussed above, phase pure $\text{Al}_2\text{O}_3\text{-TiB}_2$ powder could be formed in NaCl after 5 h firing at 1050 °C (using 30 wt% excess Al and 30 wt% excess B_2O_3), or 4 h firing at 1150 °C (using 30 wt% excess Al and 20 wt% excess B_2O_3), which was further confirmed by microstructural characterisation. Figure 7, as an example, gives TEM images of the product powder prepared under the former condition, along with the corresponding EDS, showing the coexistence of submicron-sized Al_2O_3 particles (0.3–0.6 μm) and nanosized TiB_2 particles (30–60 nm). Except these two phases, no other impurity phases were seen, as already revealed by XRD (Figure 6c). Figure 8 further displays SEM images of the product powder formed under the latter condition mentioned above. The formation of phase pure $\text{Al}_2\text{O}_3\text{-TiB}_2$ in this case was also confirmed by EDS, along with XRD (Figure 4c). However, due to the higher synthesis temperature, Al_2O_3 and TiB_2 particles in the composite powder became slightly bigger (1–2 μm Al_2O_3 and 100–200 nm TiB_2).

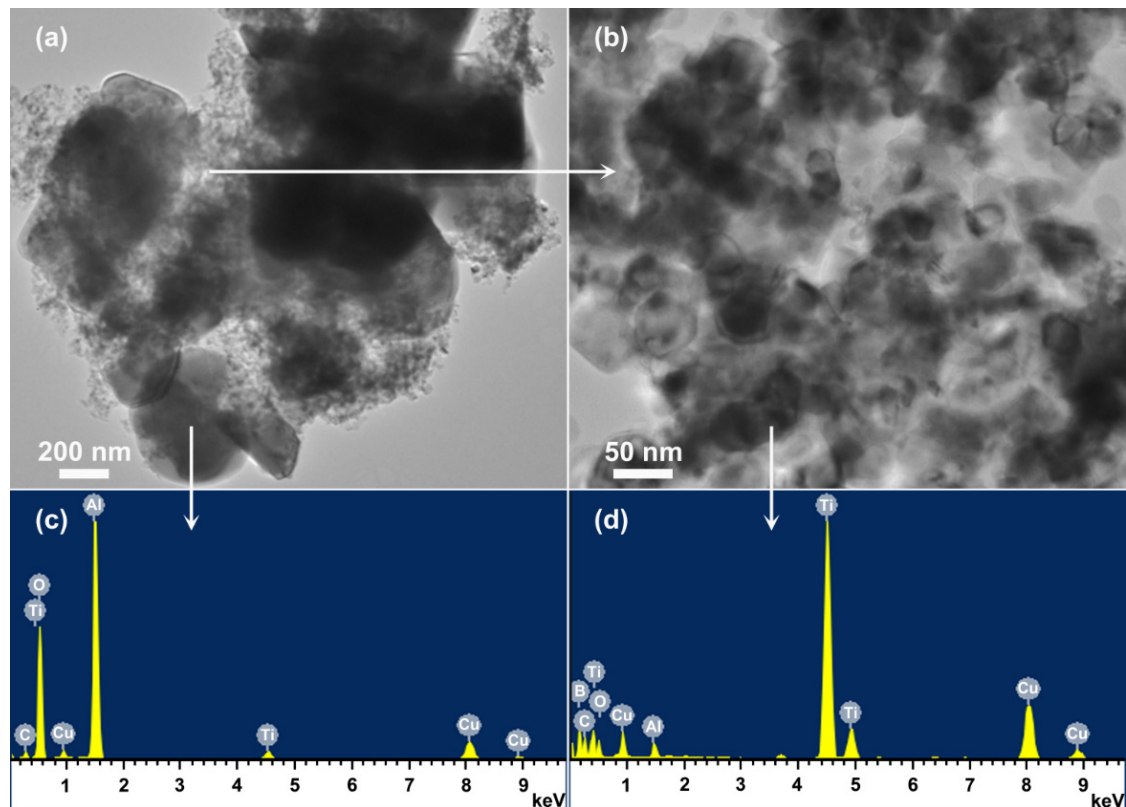


Figure 7. TEM images (a,b) and corresponding EDS (c,d) of the $\text{Al}_2\text{O}_3\text{-TiB}_2$ composite powder resultant from 5 h firing in NaCl at 1050 °C (the small C and Cu peaks arose from the carbon coating and the Cu grid).

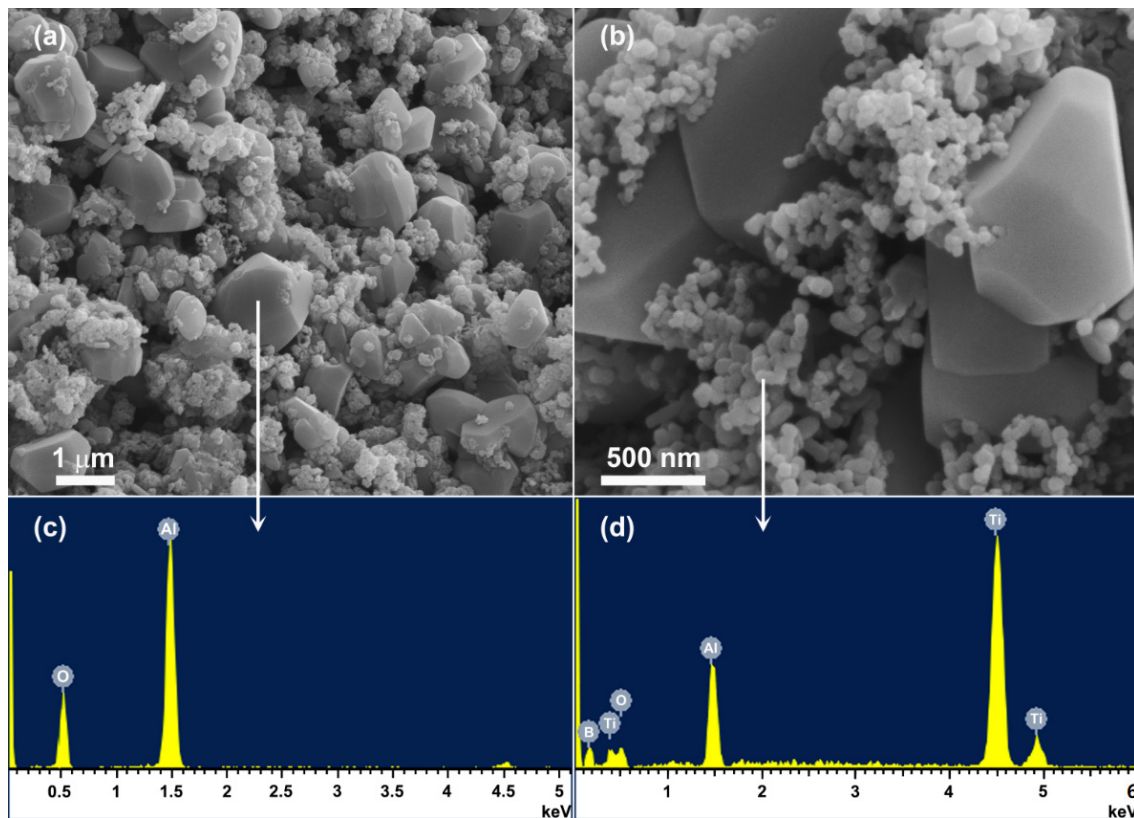


Figure 8. SEM images (a,b) and corresponding EDS (c,d) of the Al_2O_3 - TiB_2 composite powder resultant from 4 h firing in NaCl at 1150°C .

4. Further Discussion and Reaction/Synthesis Mechanism

Based on the results presented in Figures 1–8 and the preliminary discussion above, as well as on the thermodynamic calculations (Figure 9), the reaction/synthesis mechanisms (taking the case of using NaCl as an example) could be proposed; they are discussed as follows.

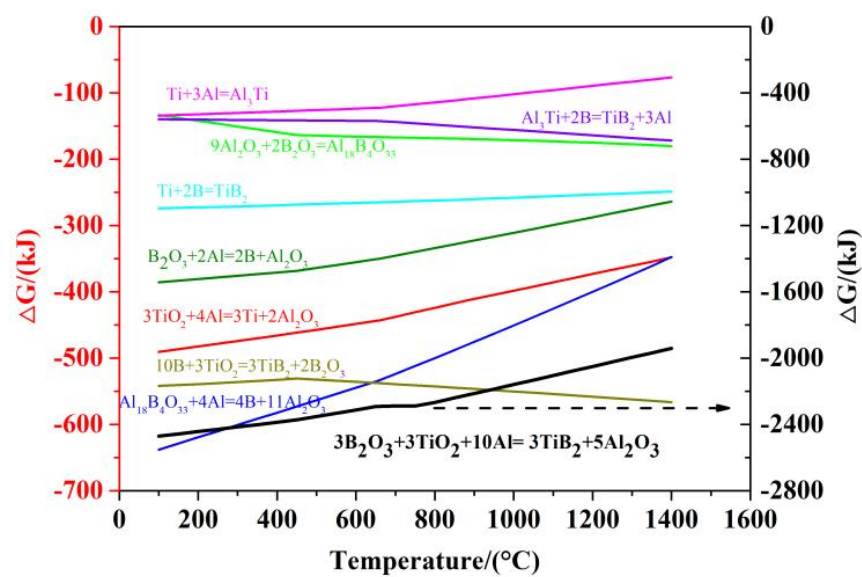
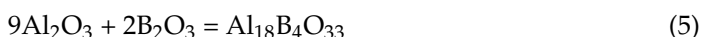


Figure 9. The standard Gibbs energy values corresponding to Reactions (1) and (3)–(10), as a function of temperature.

The firing temperatures (850–1150 °C) were above the melting points of NaCl, B₂O₃ and Al. So, at these temperatures, they all melted, forming a liquid NaCl pool, and B₂O₃ and Al liquid droplets. Then, the latter two would start to react with each other in the molten NaCl medium, forming B and Al₂O₃, according to Reaction (3).

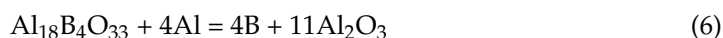
On the other hand, as discussed in our previous work on MSS of TiB₂ [39], TiO₂ also would be reduced by the Al droplets in the molten NaCl medium, forming Ti and Al₂O₃ (Reaction (4)). The Al₂O₃ formed from Reactions (3) and (4) would partially react with the unreduced B₂O₃, in the NaCl medium, forming the intermediate Al₁₈B₄O₃₃ (Reaction (5)), as detected by XRD (Figures 1–3 and Figure 5).



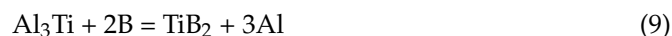
With the optimisation of synthesis condition, the intermediate Al₁₈B₄O₃₃ could be further reduced by Al in the molten NaCl, forming additional B and Al₂O₃ according to Reaction (6), as verified by XRD (Figures 3 and 5).

Apart from Al₁₈B₄O₃₃, another main intermediate phase, Al₃Ti, was formed from the reaction between the Ti formed from Reaction (4), and Al (Reaction (7)), as detected by XRD (Figures 1–6).

As discussed, and confirmed in our previous studies [37–39], the formed B and Ti (Reactions (3), (4) and (6)) were slightly dissoluble in the molten chloride salts. So, the dissolved B and Ti would diffuse through the molten salt medium and reacted with each other, forming the other desirable phase of TiB₂ (Reaction (8)).



B dissolved in the molten salt would also diffuse through the salt medium and react respectively with the Al₃Ti produced from Reaction (7), and the unreacted raw material TiO₂, forming additional TiB₂ (Reactions (9) and (10)). Reaction (9) was mainly responsible for the complete elimination of this intermediate phase under the optimal conditions (Figures 4 and 6).



As shown in Figure 9, the Gibbs energy values corresponding to Reactions (3)–(9) and the overall Reaction (1) are also negative, at test temperatures (and even at lower temperatures), suggesting that all of these exothermic Reactions are thermodynamically favourable, which further supports the plausibility of the reaction/synthesis mechanisms proposed above.

5. Conclusions

Low temperature synthesis of Al₂O₃-TiB₂ composite powders via aluminothermic reduction of TiO₂ and B₂O₃ in a molten chloride salt (KCl, NaCl or MgCl₂) was investigated. Processing parameters including salt type, initial batch composition, and firing temperature/time played important roles in the synthesis process. Phase pure Al₂O₃-TiB₂ nanocomposite powder could be prepared in NaCl after 5 h firing at 1050 °C, when 30 wt% excess Al and 30 wt% excess B₂O₃ were used. The particle sizes of Al₂O₃ and TiB₂ coexisting in the as-prepared composite powder were estimated to be 0.3–0.6 μm and 30–60 nm, respectively. By increasing the temperature to 1150 °C and using 30 wt% excess Al and 20 wt% excess B₂O₃, phase pure Al₂O₃-TiB₂ composite powder also could be prepared in

NaCl after only 4 h, although sizes of Al₂O₃ and TiB₂ particles coexisting in the resultant composite power increased slightly to 1–2 μm and 100–200 nm, respectively.

Author Contributions: Experiment and initial draft, K.B. and X.L.; conception, experiment design and thermodynamic calculation, K.B., X.L., J.C. and Q.J.; review and editing, X.L., Q.J. and S.Z.; supervision, S.Z. All authors have read and agreed to the published version of the manuscript.

Funding: This research was funded by the National Natural Science Foundation of China (Grant No. 51902180), and the EPSRC Centre for Doctoral Training in Electromagnetic Metamaterials (EP/L015331/1) at the University of Exeter.

Institutional Review Board Statement: Not applicable.

Informed Consent Statement: Not applicable.

Data Availability Statement: Data sharing is not applicable to this article.

Conflicts of Interest: The authors declare no conflict of interest.

References

- Munro, M. Evaluated Material Properties for a Sintered alpha-Alumina. *J. Am. Ceram. Soc.* **2005**, *80*, 1919–1928. [[CrossRef](#)]
- Basu, B.; Balani, K. (Eds.) Bonding, Structure, and Physical Properties. In *Advanced Structural Ceramics*; John Wiley & Sons, Inc.: Hoboken, NJ, USA, 2011; pp. 28–29.
- Williams, D. *Contemporary and Future Biomaterials*; Cambridge University Press (CUP): Cambridge, UK, 2018; pp. 475–589.
- Yazdani, B.; Xia, Y.; Ahmad, I.; Zhu, Y. Graphene and carbon nanotube (GNT)-reinforced alumina nanocomposites. *J. Eur. Ceram. Soc.* **2015**, *35*, 179–186. [[CrossRef](#)]
- Niihara, K. New Design Concept of Structural Ceramics. *J. Ceram. Soc. Jpn.* **1991**, *99*, 974–982. [[CrossRef](#)]
- Rainforth, W.M. The wear behaviour of oxide ceramics-A Review. *J. Mater. Sci.* **2004**, *39*, 6705–6721. [[CrossRef](#)]
- Chen, H.; Rainforth, W.M.; Lee, W.E. The wear behaviour of Al₂O₃-SiC ceramic nanocomposites. *Scr. Mater.* **2000**, *42*, 555–560. [[CrossRef](#)]
- Sharifi, E.M.; Karimzadeh, F.; Enayati, M.H. Synthesis of titanium diboride reinforced alumina matrix nanocomposite by mechanochemical reaction of Al-TiO₂-B₂O₃. *J. Alloys Compd.* **2010**, *502*, 508–512. [[CrossRef](#)]
- Sharifi, E.M.; Karimzadeh, F.; Enayati, M.H. Preparation of Al₂O₃-TiB₂ nanocomposite powder by mechanochemical reaction between Al, B₂O₃ and Ti. *Adv. Powder Technol.* **2011**, *22*, 526–531. [[CrossRef](#)]
- Golla, B.R.; Bhandari, T.; Mukhopadhyay, A.; Basu, B. Titanium Diboride. In *Ultra-High Temperature Ceramics: Materials for Extreme Environment Applications*; Fahrenholtz, W.G., Wuchina, E.J., Lee, W.E., Zhou, Y., Eds.; John Wiley & Sons, Inc.: Hoboken, NJ, USA, 2014; pp. 316–360.
- Kimura, I.; Hotta, N.; Hiraoka, Y.; Saito, N.; Yokota, Y. Sintering and characterization of Al₂O₃-TiB₂ composites. *J. Eur. Ceram. Soc.* **1989**, *5*, 23–27. [[CrossRef](#)]
- Liu, J.; Ownby, P.D. Enhanced mechanical properties of alumina by dispersed titanium diboride particulate inclusions. *J. Am. Ceram. Soc.* **1991**, *74*, 241–243. [[CrossRef](#)]
- Ranganath, S.; Subrahmanyam, J. Impact response of Al₂O₃ and Al₂O₃-TiB₂ ceramic composites. *J. Mater. Sci. Lett.* **1991**, *10*, 1297–1298. [[CrossRef](#)]
- Belosi, A.; De Portu, G.; Guicciardi, S. Preparation and properties of electroconductive Al₂O₃-based composites. *J. Eur. Ceram. Soc.* **1992**, *10*, 307–315. [[CrossRef](#)]
- Jianxin, D.; Xing, A.; Zhaoqian, L. Friction and wear behavior of Al₂O₃/TiB₂ composite against cemented carbide in various atmospheres at elevated temperature. *Wear* **1996**, *195*, 128–132. [[CrossRef](#)]
- Jianxin, D.; Tongkun, C.; Lili, L. Self-lubricating behaviors of Al₂O₃/TiB₂ ceramic tools in dry high-speed machining of hardened steel. *J. Eur. Ceram. Soc.* **2005**, *25*, 1073–1079. [[CrossRef](#)]
- Tampieri, A.; Belosi, A. Oxidation of monolithic TiB₂ and of Al₂O₃-TiB₂ composite. *J. Mater. Sci.* **1993**, *28*, 649–653. [[CrossRef](#)]
- Plovnick, R.H.; Richards, E. New combustion synthesis route to TiB₂-Al₂O₃. *Mater. Res. Bull.* **2001**, *36*, 1487–1493. [[CrossRef](#)]
- Stadlbauer, W.; Kladnig, W.; Gritzner, G. Al₂O₃-TiB₂ composite ceramics. *J. Mater. Sci. Lett.* **1989**, *8*, 1217–1220. [[CrossRef](#)]
- Liu, G.; Yan, D.; Zhang, J. Microstructure and mechanical properties of TiB₂-Al₂O₃ composites. *J. Wuhan Univ. Technol. Sci. Ed.* **2011**, *26*, 696–699. [[CrossRef](#)]
- Li, J.; Gao, L.; Guo, J. Mechanical properties and electrical conductivity of TiN-Al₂O₃ nanocomposites. *J. Eur. Ceram. Soc.* **2003**, *23*, 69–74. [[CrossRef](#)]
- Logan, K.V. Shaped Refractory Products and Method of Making Same. United States Patent No. 4, 891, 337, 2 January 1990.
- Ray, S.P. Boride-alumina composites: Synthesis and Fabrication. *Metall. Trans. A* **1992**, *23*, 2381–2385. [[CrossRef](#)]
- Kecskes, L.J.; Niiler, A.; Kottke, T.; Logan, K.V.; Villalobos, G.R. Dynamic consolidation of combustion-synthesized alumina-titanium diboride composite ceramics. *J. Am. Ceram. Soc.* **2005**, *79*, 2687–2695. [[CrossRef](#)]

25. Ma, Z.Y.; Tjong, S.C. In Situ ceramic particle-reinforced aluminum matrix composites fabricated by reaction pressing in the TiO₂ (Ti)-Al-B (B₂O₃) systems. *Met. Mater. Trans. A* **1997**, *28*, 1931–1942. [[CrossRef](#)]
26. Xia, T.D.; Liu, T.Z.; Zhao, W.J.; Munir, Z.A.; Wang, T.M. Photo- and cathodoluminescence of the combustion-synthesized Al₂O₃-TiB₂ composites. *J. Mater. Res.* **2000**, *15*, 1622–1629. [[CrossRef](#)]
27. Meyers, M.; Olevsky, E.; Ma, J.; Jamet, M. Combustion synthesis/densification of an Al₂O₃-TiB₂ composite. *Mater. Sci. Eng. A* **2001**, *311*, 83–99. [[CrossRef](#)]
28. Zhu, H.G.; Wang, H.Z.; Ge, L.Q.; Chen, S.; Wu, S.Q. Formation of composites fabricated by exothermic dispersion reaction in Al-TiO₂-B₂O₃ system. *Trans. Nonferrous Met. Soc. China* **2007**, *17*, 590–594. [[CrossRef](#)]
29. Zhu, H.; Wang, H.; Ge, L. Wear properties of the composites fabricated by exothermic dispersion reaction synthesis in an Al-TiO₂-B₂O₃ system. *Wear* **2008**, *264*, 967–972. [[CrossRef](#)]
30. Yeh, C.; Li, R. Formation of TiB₂-Al₂O₃ and NbB₂-Al₂O₃ composites by combustion synthesis involving thermite reactions. *Chem. Eng. J.* **2009**, *147*, 405–411. [[CrossRef](#)]
31. Mousavian, R.T.; Sharafi, S.; Shariat, M.H. Microwave-assisted combustion synthesis in a mechanically activated Al-TiO₂-H₃BO₃ system. *Int. J. Refract. Met. Hard Mater.* **2011**, *29*, 281–288. [[CrossRef](#)]
32. Mishra, S.; Gokuul, V.; Paswan, S. Alumina-titanium diboride in situ composite by self-propagating high-temperature synthesis (SHS) dynamic compaction: Effect of compaction pressure during synthesis. *Int. J. Refract. Met. Hard Mater.* **2014**, *43*, 19–24. [[CrossRef](#)]
33. Khaghani-Dehaghani, M.A.; Ebrahimi-Kahrizsangi, R.; Setoudeh, N.; Nasiri-Tabrizi, B. Mechanochemical synthesis of Al₂O₃-TiB₂ nanocomposite powder from Al-TiO₂-H₃BO₃ mixture. *Int. J. Refract. Met. Hard Mater.* **2011**, *29*, 244–249. [[CrossRef](#)]
34. Abdellahi, M.; Heidari, J.; Sabouhi, R. Influence of B source materials on the synthesis of TiB₂-Al₂O₃ nanocomposite powders by mechanical alloying. *Int. J. Miner. Met. Mater.* **2013**, *20*, 1214–1220. [[CrossRef](#)]
35. Yang, W.; Dong, S.; Luo, P.; Yangli, A.; Liu, Q.; Xie, Z. Effect of Ni addition on the preparation of Al₂O₃-TiB₂ composites using high-energy ball milling. *J. Asian Ceram. Soc.* **2014**, *2*, 399–402. [[CrossRef](#)]
36. Rabiezadeh, A.; Hadian, A.; Ataie, A. Preparation of alumina/titanium diboride nano-composite powder by milling assisted sol-gel method. *Int. J. Refract. Met. Hard Mater.* **2012**, *31*, 121–124. [[CrossRef](#)]
37. Zhang, S.; Khangkhamano, M.; Zhang, H.; Yeprem, H.A. Novel Synthesis of ZrB₂ powder via molten-salt-mediated magnesiothermic Reduction. *J. Am. Ceram. Soc.* **2014**, *97*, 1686–1688. [[CrossRef](#)]
38. Bao, K.; Liu, C.; Yazdani, B.; Damavandi, Y.; Zhang, S. Low-Temperature preparation of lanthanum hexaboride fine powder via magnesiothermic reduction in molten salt. *J. Ceram. Sci. Technol.* **2016**, *7*, 403–408.
39. Bao, K.; Wen, Y.; Khangkhamano, M.; Zhang, S. Low-temperature preparation of titanium diboride fine powder via magnesiothermic reduction in molten salt. *J. Am. Ceram. Soc.* **2017**, *51*, 257–2272. [[CrossRef](#)]
40. Li, T.; Chen, J.; Xiao, J.; Wei, Y.; Li, G.; Zhang, S.; Li, N. Formation of liquid-phase isolation layer on the corroded interface of MgO/Al₂O₃-SiC-C refractory and molten steel: Role of SiC. *J. Am. Ceram. Soc.* **2021**, *104*, 2366–2377. [[CrossRef](#)]
41. Hashimoto, S.; Yamaguchi, A. Synthesis of MgAl₂O₄ (Spinel) Powder Using MgCl₂. *J. Ceram. Soc. Jpn.* **2001**, *109*, 894–896. [[CrossRef](#)]
42. Horlait, D.; Grasso, S.; Chroneos, A.; Lee, W. Attempts to synthesise quaternary MAX phases (Zr,M)2AlC and Zr₂(Al,A)C as a way to approach Zr₂AlC. *Mater. Res. Lett.* **2016**, *4*, 137–144. [[CrossRef](#)]
43. Mousavian, R.T.; Sharafi, S.; Roshan, M.R.; Shariat, M.H. Effect of mechanical activation of reagents' mixture on the high-temperature synthesis of Al₂O₃-TiB₂ composite powder. *J. Therm. Anal. Calorim.* **2011**, *104*, 1063–1070. [[CrossRef](#)]
44. Jacobson, N.S.; Myers, D.L. High-temperature vaporization of B₂O₃(l) under reducing conditions. *J. Phys. Chem. B* **2011**, *115*, 13253–13260. [[CrossRef](#)]